PCCP

Molecular Characterization of Organic Content of Soot along the Centerline of a Coflow Diffusion Flame

Journal:	*Physical Chemistry Chemical Physics*
Manuscript ID:	CP-ART-07-2014-003330.R2
Article Type:	Paper
Date Submitted by the Author:	14-Oct-2014

Complete List of Authors:	Cain, Jeremy; University of Dayton Research Institute, Bioenergy and Carbon Mitigation Laskin, Alexander; Pacific Northwest National Laboratory, William R. Wiley Environmental Molecular Science Laboratory Kholghy, Mohammad; University of Toronto, Department of Mechanical and Industrial Engineering Thomson, Murray; University of Toronto, Department of Mechanical and Industrial Engineering Wang, Hai; Stanford University, Department of Mechanical Engineering

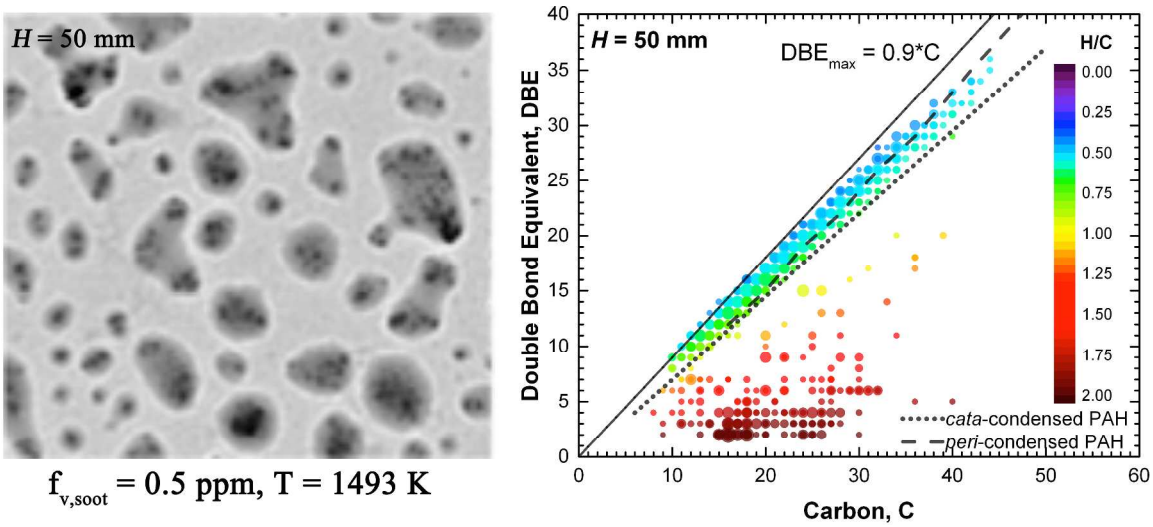

HR-MS speciation of young soot produced in a coflow diffusion flame reveal an array of 'aliphatic' and 'aromatic' $C_xH_yO_z$ constituents.

Molecular Characterization of Organic Content of Soot along the Centerline of a Coflow Diffusion Flame

Jeremy Cain,[a,†] Alexander Laskin,[b] Mohammad Reza Kholghy,[c] Murray J. Thomson,[c] Hai Wang[d]

[a] *University of Dayton Research Institute, 300 College Park, Dayton, OH 45469-0101, USA*
[b] *William R. Wiley Environmental Molecular Sciences Laboratory, Pacific Northwest National Laboratory, P. O. Box 999, MSIN K8-88, Richland, WA 99352, USA*
[c] *Department of Mechanical and Industrial Engineering, University of Toronto, Toronto, Ontario, M5S 3G8, Canada*
[d] *Department of Mechanical Engineering, Stanford University, Stanford, CA 94305, USA*

[†]Corresponding author: jeremy.cain@udri.udayton.edu

Submitted to

Physical Chemistry Chemical Physics

Abstract

High-resolution mass spectrometry coupled with nanospray desorption electrospray ionization was used to probe chemical constituents of young soot particles sampled along the centerline of a coflow diffusion flame of a three-component Jet-A1 surrogate. In lower positions where particles are transparent to light extinction (λ = 632.8 nm), *peri*-condensed polycyclic aromatic hydrocarbons (PAHs) are found to be the major components of the particle material. These particles become enriched with aliphatic components as they grow in mass and size. Before carbonization occurs, the constituent species in young soot particles are aliphatic and aromatic compounds 200-600 amu in mass, some of which are oxygenated. Particles dominated by PAHs or mixtures of PAHs and aliphatics can exhibit liquid-like appearance observed by electron microscopy and be transparent to visible light. The variations in chemical composition observed here indicate that the molecular processes of soot formation in coflow diffusion flames may be more complex than previously thought. For example, the mass growth and enrichment of aliphatic components in an initial mostly aromatic structure region of the flame that is absent of H atoms or other free radicals indicates that there must exist at least another mechanism of soot mass growth in addition to the hydrogen abstraction–carbon addition mechanism currently considered in fundamental models of soot formation.

Introduction

Soot formation is almost ubiquitous in coflow diffusion flames burning hydrocarbon fuels. Such flames are of special interest to the study of soot formation[1] because they are simpler in geometry than complex practical flames[2] and amenable to detailed modeling.[3-7] They also encompass most of the physical and chemical processes that impact soot formation.[5] Much of what is known about soot formation in coflow diffusion flames is based on laser light extinction and scattering.[1, 2, 8-10] As summarized by Glassman,[11] experimental results suggest that soot particles are generated near the high temperature regions of the flame reaction zone and are transported up the flame and towards the centerline through convection and possibly by thermophoresis. The experimental results also suggest that the rate of soot formation peaks on the fuel side at a small distance from the reaction zone. Modeling studies by Smooke, Colket and coworkers,[3, 4] Dworkin *et al.*,[12] Saffaripour *et al.*,[6, 13] and Kholghy *et al.*[7] revealed that a coupled soot model had difficulty reproducing the radial/spatial distribution of soot volume fraction even though the models were capable of reproducing the observed peak value. The models underestimate the centerline soot volume fraction and fail to predict its rapid increase along the flame centerline where the temperature is around 1500 K.

In a recent study, Kholghy *et al.*[14] examined soot volume fraction and morphology in an atmospheric-pressure laminar coflow diffusion flame of a Jet A-1 surrogate (72% *n*-decane, 18% propylbenzene, and 10% propylcyclohexane by mole). The results show that (1) particles produced along the centerline in regions where the flame is neither luminous nor allows for visible light extinction (λ = 632.8 nm) are clearly observable by transmission electron microscopy (TEM); (2) these particles that do not absorb visible light are fairly transparent to the electron beam and appear to be liquid-like; (3) detectable light extinction occurred only when the particles were observed to contain island-like, "darker" nano-sized grains that are more refractive. Figure 1 provides a schematic view of the time histories and temporal distribution of what appear to be two distinctively different types of particles. The first type is transparent to visible light (λ = 632.8 nm), and originates in the lower flame position where $T < 1500$ K.

Particles of the second type are refractive and formed in the upper part of the flame where $T \geq 1500$ K. These particles are aggregates of primary particles that are smaller in size compared to the particles convected from below and formed in relatively low temperature regions of the flame centerline (*i.e.*, $T \leq 1500$ K). It is unclear if and how these two types of particles interact with each other. The TEM results indicate mixtures of the two particle types exist, as seen in the middle TEM panel of Figure 1, prior to being convected into the high temperature regions of the flame reaction zone at higher flame heights. Kholghy *et al.*[14] suggested that the rapid increase in absorbed visible light at the flame centerline where $T \approx 1500$ K is not due to rapid particle formation or growth, but is likely caused by a change in the internal structure or chemical composition of transparent particles.

D'Anna *et al.*[15, 16] described particles that are transparent to visible radiation as nano-organic carbon particles (NOC). They used UV–visible spectroscopy and laser scattering/extinction techniques for volume fraction and particle size measurements in a Santoro co-flow laminar ethylene diffusion flame. Two types of particles were detected: soot particles (absorb light in the whole spectral range) and NOC (transparent to the visible radiation). The experimental results indicate that NOC are formed in large amounts in the central part and at the beginning of the flame, and reach a concentration comparable to that of soot particles.

The morphological transformation of the transparent particles to mature soot particles is consistent with the results reported by Dobbins and coworkers.[17-19] Those studies examined the morphology and composition of soot in laminar normal coflow diffusion flames (NDF) using normal or deuterated ethylene as the fuel and laser microprobe mass spectrometry (LMMS) to uncover the chemical evolution of soot particles. Dobbins coined the term precursor particles to distinguish young, uncarbonized particles from mature soot. Accordingly, the transition from precursor to mature particles is accomplished by carbonization.[18] Deuterated ethylene was used instead of normal ethylene to obtain unambiguous identification of PAHs ablated from soot.[19] LMMS preferentially probes refractive and thermally stable polyaromatic hydrocarbons (PAH) in particulate material. About 80% of the ions detected by LMMS were assigned as even carbon

numbered stabilomers suggested by Stein and Fahr.[20] Odd carbon numbered PAHs that were bridged with a methylene group (-CH_2-) constitute the remaining stabilomers. Benzenoid PAH stabilomers (*i.e.*, PAHs with only six membered rings) were suggested as the most important constituents of nascent soot. Stabilomers, including $C_{16}H_{10}$ (202 amu), $C_{18}H_{12}$ (228 amu), $C_{20}H_{12}$ (252 amu), $C_{22}H_{12}$ (276 amu), and $C_{24}H_{12}$ (300 amu) molecules that correspond to PAHs with four to six-membered condensed rings, were found to be the predominant fragments present in the mass spectra of precursor soot sampled below a distance of Z = 40 mm from the burner exit on the 88 mm long diffusion flame.[18] No evidence of PAH compounds was reported by LMMS in mature soot. All of its MS peaks were related to small positive ion carbon clusters (*i.e.*, ions of C_x and C_xH) characteristic of graphitic-like carbon. Based on the LMMS results, H/C ratios of 0.55 and 0.18 were measured for precursor particles at low flame heights and mature soot at higher flame heights, respectively.

PAHs measured in precursor soot correlated with those measured in the combustion gas environment. Although detectable gas-phase PAHs populate a wide range spanning from naphthalene to C_{160},[21] PAHs containing up to 32 carbon atoms are the most abundant species in coflow diffusion flames due to kinetic and thermodynamic limitations.

The morphological observation and evolution observed by Kholghy *et al.*[14] are consistent with those of Dobbins and coworkers.[17-19] Particles shown in Figure 1 are the precursor particles up to Z = 50 mm. The fact that these particles have decidedly low TEM contrast suggests that they are not carbonized. Though LMMS results suggest that the constituents of these particles are *peri*-condensed aromatics of four to seven rings in size, the result should be viewed with caution considering the inherent limitations of LMMS. Detection of less stable aliphatic compounds with LMMS is hindered by their very extensive fragmentation during laser ablation and ionization. The method does not detect volatile aromatic compounds smaller than 170 amu because they evaporate in the vacuum that the samples are exposed to during the analysis; LMMS cannot identify PAH isomers.[18] Notable uncertainties remain concerning the chemical composition of precursor particles.

Chemical and morphological properties of mature and young soot were also studied in inverse diffusion flames (IDF).[22-25] Blevins *et al.*[24] used LMMS and gas chromatography/mass spectrometry (GC/MS) analysis of PAHs extracted from precursor particles with dichloromethane (CH_2Cl_2); different isomers within the mass range of 152 to 302 amu were identified. Similar to the NDF studies of Dobbins and coworkers, the 252, 276, and 300 amu PAH stabilomers were found to be abundant in precursor soot. The mass at 202 amu was also dominant, which corresponds to fluoranthene, acephenantherene, aceanthrylene, and pyrene. The six most abundant species of the 28 targeted PAHs were pyrene, cyclopenta[cd]pyrene, fluoranthene, acephenanthrene, phenanthrene, and 4,5-methylenephenanthrene.[24]

Evidence of aliphatic structures in young soot particles has become abundant. They have been observed in a wide range of flames, including inverse diffusion flames,[22, 23, 25] counterflow diffusion flames,[26] in-cylinder diffusion flames,[27] and laminar premixed ethylene flames.[28-32] It has been suggested that the high aliphatic content is probably related to the liquid-like appearance of young soot.[24, 29-31, 33] The particles captured on the substrate borders of lacey carbon grids display surface tension effects and wetting that are characteristics of liquid-like droplets.[29, 31, 34]

The observed aliphatic structures in young soot particles are not well understood within the current level of understanding (*i.e.*, precursor particles composed of stabilomer PAHs transitioning to mature soot by carbonization). The objective of the current study is to provide further insight into the chemical composition of organic constituents in soot sampled along the centerline of the coflow diffusion flame of Kholghy *et al*.[14] These measurements will provide a more complete understanding of the precursor particles' chemical nature and the composition evolution of particles observed by TEM (Figure 1). High-resolution mass spectrometry (HR-MS) coupled with nanospray desorption electrospray (nano-DESI)[35, 36] was used for this purpose. HR-MS assisted with ambient pressure sampling and "soft" ionization is a powerful approach to provide molecular assignment of organic compounds based on the high precision detection of parent ions.[37] The technique alleviates a notable problem in a large range of mass spectrometric

approaches that rely on ‘‘hard’’ ionization, which result in severe fragmentation of aliphatic compounds and hinders their identification. HR-MS has been applied recently in aerosol science for structural characterization of individual species in complex mixtures of atmospheric organic aerosols. For example, the high-resolution spectra enabled a basic understanding of the chemical and physical processes occurring in aging of D-limonene secondary organic aerosol (LSOA).[38] This method has also been utilized to determine the sources of ambient aerosols in urban environments. For example, O'Brien *et al.*[39] performed HR-MS of ambient aerosols (2010 CalNex campaign) and SOA of isoprene and diesel fuel produced in a chamber. Due to the variation in SOA mass spectra with an organic source, they were able to determine temporal periods where these biogenic and anthropogenic sources, respectively, accounted for the composed aerosol. Similarly, Lin *et al.*[40] were able to detect organosulfates in humic-like substances in Asian aerosols, and that its origin is biogenic volatile organic compounds. The implication of our findings in this study, including chemical composition identifications, will be discussed in detail within the context of recent results in structural and chemical complexities of condensed-phase, carbonaceous materials formed in flames.

Experimental

Details of the atmospheric pressure, laminar, coflow diffusion flame of a Jet A-1 surrogate blend have been presented elsewhere.[14] Soot volume fraction, temperature, particle morphology of the same flame have also been reported earlier.[6, 13] The fuel was a 3-component mixture of *n*-decane, propylbenzene and propylcyclohexane, with component mole percentages of 72%, 18% and 10%, respectively. Figure 2 shows the experimental flame setup. The inner and outer diameters of the burner's steel fuel tube are 10.9 mm and 12.7 mm, respectively. The air annulus has an inner diameter of 90 mm. Protecting the flame from air perturbations is accomplished by a clear acrylic tube 152.4 mm in diameter (ID) and 304.8 mm in height. Air circulation inside the enclosure was avoided by a ceramic honeycomb on top of the chimney. Access holes in the acrylic tube for the thermophoretic sampling probe are also shown in Figure

2. The burner sat on a manual translation stages to allow accurate positioning (spatial accuracy of $\pm$ 0.01 mm) in horizontal and vertical directions.

The fuel mixture was diluted with nitrogen and vaporized at 463 K using a controlled vapor delivery system (Bronkhorst, model W-102A). Heated tubes maintained at 500 K transfer the fuel to the burner. To prevent fuel condensation in the fuel tube inside the burner, the coflow air is heated to 423 K and the last two inches of the fuel tube are kept at 473 K using thin flexible heaters (Minco). The fuel and carrier gas (N_2) flow rates were 14.3 g hr^{-1} ($\pm$1%) and 0.81 L min^{-1} ($\pm$ 5% at 293 K), respectively. The flow rate of the coflow air was 55 L min^{-1} (at 294 K). Additional oxygen (3 L min^{-1} at 294 K) was added to the coflow air to prevent flame lift-off due to high dilution. The resulting visible flame height was about 80 mm, with a lift-off of less than 1 mm.

Soot particles were removed from the flame centerline using thermophoretic sampling onto aluminum foil substrates in a technique similar to those of previous studies.[14, 42, 43] A schematic of the sampling apparatus is shown elsewhere.[6] There is a 10 mm (width) $\times$ 80 mm (height) access port on the acrylic tube that is used for thermophoretic sampling. Space between the access port and sampling probe perimeters is sealed to avoid air current perturbations. The foil substrates are custom made to 4 mm *x* 4 mm square shape from general purpose aluminum foil (MacMaster Carr, 9060K51). The substrate is held between two 0.3 mm thick stainless steel sheets on the 40 mm long sampling probe. Thus, perturbation to the flame due to the occupied thermopheretic sampling volume is small: 5% of the differential flame volume is occupied by the sampling unit during insertion. The holder is attached to a double acting pneumatic air cylinder (bore = 2.70 cm, stroke = 2.54 cm) that is actuated by two high flow rate solenoid valves (3/2-way, normally closed) operating at 45 psi. To synchronize the motion of the piston, the timer function of an Omron ZEN V2 programmable logic controller (PLC) is used. The exposure time was slightly less at 60 mm sampling height (45 ms) than at lower heights (60 ms for 30, 40, and 50 mm); values were chosen to provide adequate sample loadings for the analysis method. To minimize the unavoidable substrate contamination when it is passed through the flame to arrive

at its desired location, the travel time was kept below 10% of the exposure time. Multiple insertions (typically 3–6) were performed to accumulate enough mass on the sampling substrate. More insertions were needed at low flame heights compared to high flame heights due to the smaller thermophoretic force (lower temperature gradient between flame gas and substrate) and, consequently, less mass accumulation on the sampling substrate during each insertion. Sampling at the flame centerline was chosen because the lower temperature gradients there allow the particle evolution to occur over a longer length scale; larger gradients along other streamlines cause the process to occur over shorter lengths.[14] Thus, sampling along the flame centerline provides samples that are least affected (*i.e.*, most uniform) by the sampling substrate.

Organic components of soot samples collected on the aluminum substrates were probed using high-resolution mass spectrometry coupled with a nanospray desorption electrospray source described elsewhere.[35, 36] Briefly, the nano-DESI probe was comprised of two fused-silica capillaries (OD = 0.193 mm, ID = 0.100 mm) with polyimide coating (Polymicro); the capillaries are adjacent with a liquid bridge connecting them. Solvent was pumped through the primary capillary to the liquid bridge over the analyte, and was subsequently transferred into the nanospray capillary that fills up by capillary action and empties by electrospray. A potential difference (~4 kV) between the two capillaries maintains the solvent flow, which was supplied at ~ 0.6 μL min^{-1}. Mass spectra were obtained using an LTQ Orbitrap mass spectrometer (Thermo Scientific) operated in negative ion mode with a resolving power of 100,000 $m/\Delta m$ at m/z = 400. The solvent used in this study was a 70/30 (by volume) acetonitrile/toluene mixture. The instrument was calibrated prior to measurements with a standard calibration mixture up to a mass of 2000 amu. (MSCAL 5, Sigma-Aldrich, Inc.). The aluminum foil strips containing samples were taped to a glass slide and rastered below the liquid bridge using a programmable stage.[36] Measurements were performed in the following manner: 1) rastering the solvent bridge over a sample-free area of the substrate to obtain a background signal (~ 2 min), 2) removing bridge contact with the foil to re-position the substrate at desired location (~ 1 min), 3) resuming contact

with the foil and rastering in the sample-loaded area of the substrate (~ 5 min), and 4) removing contact with the foil to clear the nanospray capillary of sample (~ 4 min).

The mass spectra were processed in the following manner to determine the chemical composition and structure of measured species. Spectra of the background and samples were averaged over the data acquisition time. Spectral features with a signal-to-noise ratio greater than 5 were extracted from the spectra using Decon2LS software (http://ncrr.pnl.gov/software/) developed at Pacific Northwest National Laboratory (PNNL). Data processing was performed using a suite of Microsoft Excel macros also developed by the PNNL group and described elswhere.[44] The peaks corresponding to ^{13}C isotopes were removed before the background and signal peaks lists were aligned to remove the background peaks from the list. Peaks with the same *m*/*z* (background and sample) that have an intensity ratio (sample/background) greater than 2.5 were retained, while all others were removed. The remaining peaks were then grouped using first- (CH_2) and second-order (H_2) mass defect analysis,[44] which enabled clustering of the two-dimensional homologous series of peaks separated by the number of CH_2 and H_2 units into distinctive groups. This method allows all members of the group to be identified by identifying only one member of the group; it greatly simplifies the analysis for the many species observed in HR-MS data. Elemental formulas were assigned to one peak in each group using MIDAS molecular formula calculator (http://magnet.fsu.edu/~midas/). The following constraints were used in the molecular formula assignments: $C \leq 60$, $H \leq 100$, $O \leq 20$, $N \leq 1$, $S \leq 1$. Neutral formulas were obtained by adding a proton to the formulas of $[M–H]^-$ species. The double bond equivalent (DBE) was calculated from the molecular composition to determine its structural bonding.[45, 46]

It should be noted that electrospray ionization is biased towards detection of oxygenated and other polar compounds, and is inefficient for detection of pure hydrocarbons. Polar compounds have frequently been observed in soot,[30] and are observed in the organic content of soot particles here. Thus, although the method cannot detect all of the samples' organic constituents, it can be used to characterize and assign unambiguous formulae to hundreds of

compounds in each sample (1004 different $C_xH_yO_z$ species were assigned over all four heights). The strong advantage of nano-DESI is a soft ionization process that preserves original analyte molecules from fragmentation and, thus, allows detection of originally ionized molecules. Also, in the context of this study the presence of oxygen in all assigned species might be a result of both 'in flame' and 'post sampling' oxidation that modifies the original analyte material. However, oxidized species is expected to preserve most of their carbon skeletons and allow assessment of their evolving C/H ratios to be indicative of the original molecules' chemical structures, as presented in this paper.

Results

Mass spectra of the particulate matter samples were collected along the flame centerline at four heights (z = 30, 40, 50 and 60 mm), as shown in Figure 3. Data indicate a definitive overall trend in the mass spectra as the flame height increases. From z = 30 to 50 mm, the distribution of mass peaks shifts to slightly larger m/z values with the higher end of the spectrum being more populated. This signifies size growth of constituent species as the particles are convected up in the flame. A large amount of peaks were detected in the m/z range of 150–1000 Da, with a substantial amount (82–92%) occurring below 600 Da. Due to the increased amount of potential assignments and relatively small amount of species detected above 600 Da, analysis is restricted below 600 Da. Based on the mass accuracy and resolution used in the current study, we were able to provide unambiguous assignment for ~60% of the 150–600 Da peaks with $C_{0\text{-}60}H_{0\text{-}100}O_{0\text{-}20}N_{0\text{-}1}S_{0\text{-}1}$ formulas, and the remaining portion (~40%) was unassigned. Most of the assigned peaks have $C_xH_yO_z$ formulas (50%), while small fractions of peaks were also assigned as $C_xH_yO_zN_1$ (3%) and $C_xH_yO_zS_1$ (6%) compounds. Thus, the fraction of all detected peaks assigned a $C_xH_yO_z$ formula are 48, 53, 35 and 44% at heights of 30, 40, 50 and 60 mm, respectively. Although a substantial number of peaks contain N_1 and S_1 signature, the elemental fraction of both N and S is less than 1000 PPM. Appearance of N_1- and S_1-containing organic species is likely a result of trace impurities in the hydrocarbon blend. N_1-compounds might be

also related to minor reactions with nitrogen oxides in the flame. In this manuscript we limit our analysis and discussion only to the CHO species.

Particle chemical composition may be analyzed first by examining the variation of the number of H atoms with respect to the number of C atoms identified in individual constituent species. Figure 4 shows the results for the CHO species detected at the four flame heights. Several limits are shown for data assessment purposes: saturated aliphatic hydrocarbon limit ($H = 2C + 2$) – blue line, *cata*-condensed PAHs ($H = 0.5C + 3$) – dashed read line, and *peri*-condensed PAHs ($H = (6C)^{0.5}$) – solid red lines.[47] Given that the CHO species are distributed between the aliphatic and aromatic limits with apparent clustering at the areas close to the limiting cases, a separation line of $H = 1.25C + 2.5$ (midway between the aliphatic and the *cata*-PAH limits) was chosen to formally distinguish between "aliphatic CHO" (blue symbols above the line) and "aromatic CHO" (red symbols below the line) species.

Figure 4 clearly shows that the species detected fall in two separate bands: the PAH band (red) and the aliphatic band (blue). The few points that lie between the two bands (*i.e.*, close to the class separation line) are alkylated aromatics, with a hydrogen-to-carbon ratio of 1.0 – 1.5. The number of inter-band species increases with an increase in height. Overall, the data indicate that the detected species in all soot samples are composed of aliphatic and aromatic mixtures. Of particular interest is that the mass spectra do not show any C-H combinations that are indicative of the fuel components ($C_{10}H_{22}$, C_9H_{18} and C_9H_{12}) or fragments reminiscent of the fuel components. This observation rules out the possibility of fuel condensation on the soot sample.

It is observed from the plots that the dominant species change from aromatic CHO to aliphatic CHO as the height increases. The aromatic fraction of species dominates at the lowest height (30 mm) while aliphatic species become more abundant at 40, 50 and 60 mm. With increasing height, the size range of the aromatic species broadens in the samples collected between 30 mm and 50 mm heights, but then shrinks back significantly in the sample collected at 60 mm. The shift in size of the aromatic species to larger carbon numbers is likely due to PAH ring growth within the flame. The cause for its shift back to smaller carbon numbers at 60 mm is

287 illusive. It is plausible that growing PAHs at that point start to form carbonized, graphitic-like
288 material that would be undetectable by nano-DESI/HR-MS analysis. As shown in Figure 1, 60
289 mm is the first location on the flame centerline where only mature soot particle with graphitic-
290 like structure are observed. Graphitic-like material is less solvent-extractable and less ionizable.
291 Aliphatic-like species span approximately the same size range in all four samples. They become
292 more abundant as the height increases, despite the fact that the particles at the highest position
293 analyzed appear to be quite carbonized (inferred from the TEM image[14] shown in Figure 1).
294 A statistical analysis of CHO composition was carried out to further show their chemical
295 variations. Histograms of carbon number and ratios of hydrogen-to-carbon and oxygen-to-
296 carbon are shown in Figure 5 for aromatic CHO and aliphatic CHO compounds. The values are
297 plotted on the basis of frequency and summed peak intensity. Size trends of aromatic and
298 aliphatic species at different sampling heights previously discussed for Figure 4 are readily
299 observed in the plots for carbon number. The size of the aromatic species is typically around 20
300 carbon atoms. The sizes increase slightly from z = 30 mm to 40 mm, and then decreases at
301 higher heights. The number of carbon atoms in aliphatic components is somewhat more
302 narrowly distributed than that the aromatic species. The total intensity of the aliphatic species is
303 small in comparison to that of the aromatic species at z = 30 mm; but it increases and catches up
304 to the level of the aromatic species at z = 60 mm. The results suggest that a majority of the
305 constituent species in the particle are aromatic in nature at lower height and the aliphatic-to-
306 aromatic ratio increases with an increase in flame height. Another interesting observation is the
307 persistent zig-zag feature in the intensity sum for aromatic CHO species; the higher intensity
308 values are largely associated with an even number of C atoms. In contrast, this feature is
309 significantly less pronounced for aliphatic components.
310 With respect to the H/C ratio, the distributions of aromatic species show a mean value of
311 H/C ~ 0.6 with a small shoulder becoming more prominent with increased height. Aliphatic
312 species have higher H/C ratios than aromatic compounds, which all exhibit a broad range of 1.4
313 < H/C < 2.0 with a mean value of approximately 1.7; no apparent maximum is seen in the

frequency-based distributions. As previously discussed, the particles sampled at the lowest position (z = 30 mm) show very little aliphatic presence, and the dominant constituents are PAHs with size ranging from 10 to 30 carbon atoms and an H/C ratio around 0.6. The summed intensity-based H/C ratio distributions of both aromatic and aliphatic species have similar overall shapes as their frequency-based counterparts. However, the summed intensity-based distributions show higher abundances for the aromatic species with H/C in the range of 0.7-1.4, indicating higher intensity of individual MS peaks. Trends in the distributions of the O/C ratios point to most apparent values of 0.1 to 0.2 for aromatic species and 0.2 to 0.3 for aliphatic species without major differences between 30, 40 and 50 mm samples. Higher O/C ratios are observed for the sample at 60 mm.

A plot of the H/C ratios as a function of the species mass is indicative of the variation of the molecular composition as a function of the molecular size. Using the number of hydrogen in the molecule as the color scheme, Figure 6 shows these variations, where the dashed line indicates the separation of the aliphatic and aromatic components. Slight downward-sweeping asymptotic bands of similar hydrogen number in the species (similar color) are seen for the aromatics (the lower band of symbol with colors ranging from blue to yellow). The lower limit of the band represents the *peri*-condensed, stabilomer sequence and is quite cleanly defined as one would expect. For example, values of H/C = 0.625, 0.5, 0.4375 and 0.38 correspond to pyrene (202 amu), coronene (300 amu), ovalene (398 amu) and circumcoronene (520 amu), indicating the abundant presence of the most stable form PAHs in the samples analyzed for all positions, in agreement with Dobbin's LMMS observations.[17] The upper end of the aromatic band are probably *peri*-condensed PAHs with different degrees of alkylation. The aliphatic band lies roughly above the dashed line with the maximum H/C ratio equal to ~2. These are clearly saturated alkane species. Aliphatic species with H/C ratios smaller than 2 are also quite abundant, indicating that many of the aliphatic groups may contain double C–C bonds.

The distinct bands of aliphatic and aromatic CHO species depicted in the H/C plots are correlated with molecular structure in the double bond equivalent (DBE) plots of Figure 7.

These plots show a band of aromatic species in which the number of DBE increases with an increase in molecular size. The average degree of unsaturation for aromatic species was calculated as 14.9 (30 mm), 17.0 (40 mm), 17.5 (50 mm) and 13.1 (60 mm). The *peri*- and *cata*-condensed PAHs are denoted by the dashed and dotted lines, respectively; the solid line denotes the theoretical maximum DBE value for oxygen-free PAHs.[46] The aliphatic components, however, does not have this well defined structure. They typically contain two to seven DBE, which increases slightly towards higher heights, and the number of double bonds does not vary systematically as a function of the molecular size. The average degree of unsaturation for aliphatic species was calculated as 3.2 (30 mm), 3.5 (40 mm), 3.4 (50 mm) and 3.3 (60 mm).

Oxygenates were abundant in all soot samples. Figure 8 shows the variations of the O/C ratios to the species molecular mass. The ex situ nature of the measurement must be kept in mind to understand the data. The samples have been exposed to the high-temperature oxidizing region of the flame during particle sampling and later to ambient air. The measurement is not directly indicative of the oxygenated species nature of the particle constituents; rather, the data show the tendency to oxidation for different constituent species in the particle. Species containing up to 10 oxygen atoms have been detected, with most of the species containing one to six oxygen atoms. Another informative way to present the O/C data is with the van Krevelen plots shown in Figure 9. The cluster of points around H/C ~ 0.6 are the aromatic species, and those with H/C > ~1.3 are aliphatics. Two observations can be made about the data. First, it appears that there is no correlation between the H/C and O/C ratios for aliphatic species. These ratios, however, follow a linear relationship for aromatic species. Thus, the amount of oxygen in aromatics is proportional to the hydrogen content. Aromatic species range from slightly oxidized high DBE molecules (high C, low H) to higher oxidized lower DBE species (lower C, higher H). Second, aliphatic compounds are concentrated toward higher O/C values than aromatic molecules. Aromatics span a wide range of O/C ratios while aliphatics span a shorter range at higher O/C ratios. Examination of the data shows that the amount of oxygen in aliphatic species is approximately proportional to the H/C ratio.

Lastly, four types of chemical structures may be identified from the chemical analysis, as shown in Figure 10. They range from species containing one-ring aromatics to multi-rings and large *peri*-condensed PAHs, as well as pure aliphatic components. Most of them are oxygenated even though it remains unclear whether these oxygenates are the result of in situ or ex situ chemical processes. The specific chemical structures depicted in the figure are only plausible due to the various isomers. However, the four distinctive types are definitive from the observed H/C ratios and DBE values.

Discussion

Upon comparing previous TEM imaging[14] (Figure 1) and HR-MS results, it is clear that the liquid-like particles produced along the centerline at the base of the flame are aromatic in nature. These particles are composed mostly of *peri*-condensed PAHs, with some of them being alkylated. These particles are transparent to visible light at 632.8 nm and, thus, the lack of light extinction is not a direct consequence of aliphatic presence in the particle. Rather, the degree to which the particles extinct light is uncorrelated with the aliphatic content in the particles. Significant aliphatic content observed in particles at z = 40 mm and the homogeneous contrast within the particle grain (TEM observation) at the same position suggest that the aliphatic and aromatic components are well mixed during that stage of particle size/mass growth. Moreover, the particles formed early and composed mainly of PAHs appear to serve as "seed" particles for the aliphatic growth.

The two-phase material observed at z = 50 mm clearly contains graphitic grains, but the composition measurements made here do not reveal any qualitative chemical transformation that may have occurred at that height. The solvent extractable species have the largest mean size, and the size and composition distributions are also the widest. The evolution of the molecular size, composition, and especially the aliphatic-to-aromatic ratio appear to be continuous and smooth without indication of any sudden change. Hence, two possible mechanisms may be advanced to explain the two-phase material observed earlier. The first mechanism involves carbonization

within the liquid-like particles leading to the dark grains inside the liquid-like structure, as seen in the TEM analysis.[14] The second possibility is coalescence of the liquid-like particles with smaller, more graphitized particles formed in the annular region of the flame that are transported up (convection) and inward (thermophoresis). If this is the case, the particles convected into the flame have two separate origins and time-temperature histories. The mechanistic and kinetic interplay between the two material phases within the particles during their carbonization remains to be unclear. It is also perplexing that there are relatively large aliphatic components observed at z = 60 mm, where the TEM images[14] appear to show quite graphitized aggregate particles. The narrowed molecular size and H/C ratio distributions suggest that condensed-phase carbonization does occur and such processes are accompanied with the disappearance of the large aromatic species.

The above findings are consistent with the results reported by Reilly *et al.*,[48] who studied the physical and chemical evolution of particles sampled from a mid-height cross section of an acetylene laminar coflow diffusion flame using real-time aerosol mass spectrometry (RTAMS). RTAMS enabled direct observation of the carbonization process' evolution, determination of the degree of carbonization for each measured particle, and measurement of the size distribution of particles. Two types of soot particles were detected and categorized based on the mass spectra. In the low-mass spectra, peaks separated by 12 amu originate from C_nH and C_nH_2 and are attributed to mature soot particles. PAH-containing soot particles are recognized by CH_n peak separations in the high-mass region. No correlation between particle size and composition was observed. Oxygenated and hydrocarbon fragment ions are also observed in the low-mass region.

The measurements reported herein suggest that soot formation in coflow diffusion flames may be more complex than previously thought. This is especially true at lower flame heights. The role of aliphatic components and their contribution and influence to the size and mass growth, as well as later oxidation and carbonization, currently remain unclear. Presumably, uncarbonized molecular constituents (especially aliphatic components) undergo competitive oxidation and carbonization. The amount of species in the size range of 200-600 amu that

survive the oxidation (or even evaporation/thermal decomposition) is not known. It is clear, however, that the different chemical structures depicted in Figure 10 should have different kinetic mechanisms and rates for both oxidation and carbonization.

The detection of a significant amount of aliphatics is not surprising, despite the fact that the nano-DESI/HR-MS technique can be sensitized to the detection of aliphatics. For example, aliphatics have been observed in soot samples from an IDF in a series of works reported by Santamaria *et al.*[22, 23, 25] They studied the chemical composition of soot collected at different heights of benzene and ethylene IDFs using FT-IR and ^{1}H NMR; both techniques are sensitive to aliphatic components. Considerable amounts of chloroform-extractable material showed significant content of aliphatic structures and oxygenated species for both precursor and mature soot.[23] For the ethylene flame, the chloroform-extractable content was 95% and 50% for precursor and mature soot, respectively.[23] The amount of extractable material from the liquid-like soot particles near the fuel tube mouth was significantly higher than mature soot produced higher in the flame (both flames). NMR results indicated large aliphatic chains or unsaturated rings (naphthenic-type) joined to different types of aromatic rings at these flame heights.

Traces of aliphatic-bridged structures and oxygenated species are also observable in the chemical composition of soot produced in counterflow diffusion flames.[26] Skeen *et al.*[26] measured the mass spectra of particles and condensable species sampled from counterflow diffusion flames of acetylene, ethylene and propane using photoionization aerosol mass spectrometry. Low molecular weight radical species such as CH_3, C_2H_5, C_3H_2, C_3H_3, C_3H_5, C_4H_5, C_5H_3, C_5H_5 and C_6H_5 were observed in the mass spectra of sampled particles or condensed matter. These are presumably radical fragments produced during fragmentation and ionization of the particle material as side chains bonded to small aromatics and PAHs. Based on the contrasting mass spectra characteristics of samples from flames burning different fuels, they suggest that the chemical composition of soot precursor species is a function of the fuel chemical structure.

A recent study of diesel engine combustion particles also reveals the presence of aliphatic functional groups in soot's chemical composition. Wang *et al.*[27] studied the surface functional groups and oxidation reactivity of these diesel particulates. Aliphatic C-H groups on the soot surface were clearly observed during the early stage of particle formation but are lost in the premixed combustion phase, where the ratio of aromatic C=C to aliphatic C-C increases rapidly. This ratio continues to increase during the diffusion combustion stage.

All of the aforementioned findings about the presence of aliphatic components in soot samples are also consistent with observations made in the post flame region of laminar premixed ethylene flames,[28-32] as well as structural inhomogeneity observed by the newly available helium ion microscopy.[49, 50] Under less defined flame conditions, the organic and graphitic constituents in soot emitted from the flame can vary widely depending on the flame conditions. For example, the composition of soot emitted from underventilated[51] and overventilated[52] flames have been studied. Particles from an underventilated flame are precursor-like in structure and are up to 53% organic and 47% graphitic. However, soot from overventilated flames is carbon-like and is only 4% organic. It should be noted that the organic components mentioned here can be both aliphatic and aromatic, but the transformation from precursor particles to graphitic carbon in non-premixed flames appears to be universal irrespective of the flame conditions and geometry.

The above discussion points to the fact that there can be significant variations between particle morphology and chemical composition as it evolves in the flame. It is critical to note that the current soot formation models have yet to account for the wide range of variations in particle composition. For example, most of these models do not consider the role of aliphatic components and growth because the conceptual advance of these models was made prior to researchers' ability to probe the composition of growing particles. Moreover, light extinction measurements performed at a single wavelength are not expected to yield accurate information about the evolution of the particle volume fraction because of the variation in extinction coefficient as a function of the particle chemical composition and age.[7, 15]

Lastly, we comment on plausible mechanisms for the observed mass and size growth of the "precursor" or "transparent" particles along the centerline of the flame below 1500 K (region in which $z < 50$ mm). It was discussed earlier that the particles at $z = 30$ mm are composed mainly of PAHs. From that flame position, these particles appear to undergo mass/size growth with a preferential increase in the aliphatic content. Figure 11 shows the centerline temperature and mole fraction profiles computed earlier for gas-phase species of interest.[6] The concentration computed for pyrene at $z = 30$ mm is around 10^{-5}, a level high enough to cause particle inception based on the current mechanism and models of soot formation.[53, 54] As expected, the H-atom concentration is negligible below $z = 50$ mm as the temperature is too low to sustain radical chain reactions. Based on the HACA mechanism and under the condition along the flame centerline, the surface reaction rate is proportional to the H atom concentration. At 1500 K the time constant for the growth of two carbon atoms on a soot particle is estimated to be > 60 ms if the mole fraction of the H atom is below 10^{-5}. Yet for $30 < z < 50$ mm, the total flow time is smaller than 100 ms. Thus, the mass growth observed over the same range of spatial distance cannot be driven by the HACA mechanism. The same conclusion has been reached earlier in an analysis of a premixed ethylene flame at the equivalence ratio of ~2.5, in which soot was observed to sustain its mass growth in the post flame region without the presence of H atom or other radicals.[28, 33] The aliphatic components are covalently bonded with the aromatic units since van der Waal type bonding would be too weak to allow their survival at the prevailing temperature. These facts suggest that there exist persistent free radicals in the particles just nucleated out of gas phase at around $z = 30$ mm. Such a suggestion has been made earlier,[33, 55] but little is known about the origin of or the molecular structures associated with such free radicals. Delinger and coworkers[55] proposed that these radicals are resonantly stabilized and have molecular structures containing semiquinone or phenoxyl, while others suggested molecular-strain induced weakly bound carbon-carbon structures that can produce free radicals dynamically.[56] Such radicals have also been considered as the source of sustained free radical

generation by inhaled airborne particulate matter.[57] Unfortunately, direct experimental data is currently unavailable to shed further light on this problem.

Related to the plausible mechanism is the nature of growth species. As seen in Figure 11, below $z \approx 45$ mm the dominant species are C_2H_4, H_2, and CO (in addition to H_2O and CO_2). For $30 < z < 40$ mm, the concentration of C_2H_2 is almost an order of magnitude lower than that of C_2H_4. Thus, the growth of the aliphatic components in that range of the flame is the most likely driven by C_2H_4, CO and H_2. It is interesting to note that in premixed flames of ethylene-oxygen-argon in which nascent soot of a similar nature was observed, the potentially relevant, dominant species are C_2H_2, CO and H_2. Hence, the mass growth of precursor soot in the lower position of the diffusion flame below 1500 K considered herein and the post flame region of premixed flames discussed above could be the result of reactions of C_2H_2 or C_2H_4 over the surface radical sites, followed by hydrogenation by H_2. Alternatively, CO and H_2 could also be the reactants in a mechanism similar to the Fischer-Tropsch process (in which they convert to aliphatics over a catalyst), with the previously formed aromatic core acting as the catalyst.

Conclusion

The chemical composition of young soot particles along the centerline of a coflow diffusion flame of a three-component Jet-A1 surrogate are examined in detail using high-resolution mass spectrometry coupled with nanospray desorption electrospray ionization. These young particles, which still undergo mass and size growth and condensed-phase chemical transformation, differ from mature soot notably as revealed from earlier TEM and light extinction measurements.[14] The critical results of this investigation include the following:

(1) In lower positions where the particles are first detected by TEM but not by light extinction, the particles are composed mainly of *peri*-condensed PAHs that are characteristic of Stein's stabilomers, though some of these species are alkylated;

(2) Young soot particles observed in the coflow diffusion flame can be rich in aliphatic species in addition to aromatics;

(3) Prior to carbonization, the constituent species in young soot particles are composed of aliphatic and PAH compounds 200-600 amu in mass. Some of them can be oxygenated;

(4) The liquid-like appearance of young soot observed by TEM is not the direct consequence of aliphatic constituent molecules. Particles dominated by PAHs or mixtures of PAHs and aliphatics within 200-600 amu can both exhibit this behavior. Both appear to be transparent to visible light;

(5) The variations in chemical composition discussed here indicate that the molecular processes of soot formation in coflow diffusion flames may be more complex than previously thought.

The current study indicates that further experimental work is needed. Such studies must combine a range of experimental techniques (*e.g.*, microscopy, light extinction and scattering at different wavelengths, and chemical composition measurements) in order to obtain a full quantitative picture of the particle nucleation and growth processes. With simpler fuels and measurements that can follow the spatial time evolution of particle size and composition (especially around the base of the flame, in middle regions of the flame at and around heights where the two-phase material begin to appear and transform into aggregates), it may be possible to put together a more accurate mechanistic picture for soot nucleation, growth and chemical transformation in coflow diffusion flames.

Acknowledgements

The work at EMSL/PNNL was supported by the Chemical Imaging Initiative of the Laboratory Directed Research and Development program at the Pacific Northwest National Laboratory (PNNL). The nano-DESI/HR-MS analysis was performed at Environmental Molecular Sciences Laboratory, a national scientific user facility located at PNNL and sponsored by the Office of Biological and Environmental Research, U.S. DOE. PNNL is operated by the U.S. Department of Energy by Battelle Memorial Institute under contract DE-AC06-76RL0. This research was performed in part while Jeremy Cain held a National Research Council Research Associateship Award at Wright-Patterson Air Force Base. Support from the UDRI Shock Tube Lab is also appreciated. Work at Stanford was supported by the Combustion Energy Frontier Research Center (CEFRC), an Energy Frontier Research Center funded by the U.S. Department of Energy, Office of Science, Office of Basic Energy Sciences under Award Number DE-SC000119. Work at the University of Toronto was supported by the Natural Sciences and Engineering Research Council of Canada (NSERC) and BiofuelNet Canada. Mohammad Reza Kholghy also acknowledges the NSERC Vanier program for a graduate scholarship and Dr. Meghdad Saffaripour for discussions.

References

1. R. J. Santoro, H. G. Semerjian and R. A. Dobbins, *Combust. Flame*, 1983, **51**, 203-218.
2. R. J. Santoro, T. T. Yeh, J. J. Horvath and H. G. Semerjian, *Combust. Flame*, 1987, **53**, 89-115.
3. M. D. Smooke, C. S. McEnally, L. D. Pfefferle, R. J. Hall and M. B. Colket, *Combust. Flame*, 1999, **117**, 117-139.
4. C. S. McEnally, A. M. Schaffer, M. B. Long, L. D. Pfefferle, M. D. Smooke, M. B. Colket and R. J. Hall, *Symp. (Int.) Combust.*, 1998, **27**, 1497-1505.
5. F. Liu, H. Guo, G. J. Smallwood and Ö. L. Gülder, *Combust. Theor. Model.*, 2003, **7**, 301-315.
6. M. Saffaripour, A. Veshkini, M. Kholghy and M. J. Thomson, *Combust. Flame*, 2014, **161**, 848-863.
7. M. Kholghy, J. Weingarten and M. Thomson, *P. Combust. Inst.*, 2014, in press, doi: 10.1016/j.proci.2014.1007.1019.
8. B. S. Haynes and H. G. Wagner, *Ber. Bunsenges. Phys. Chem.*, 1980, **84**, 499-506.
9. J. H. Kent, H. Jander and H. G. Wagner, *Symp. (Int.) Combust.*, 1981, **18**, 1117-1126.
10. J. H. Kent and H. G. Wagner, *Combust. Flame*, 1982, **47**, 53-65.
11. I. Glassman, *Symp. (Int.) Combust.*, 1989, **22**, 295-311.
12. S. B. Dworkin, Q. Zhang, M. J. Thomson, N. A. Slavinskaya and U. Riedel, *Combust. Flame*, 2011, **158**, 1682-1695.
13. M. Saffaripour, M. Kholghy, S. B. Dworkin and M. J. Thomson, *P. Combust. Inst.*, 2013, **34**, 1057-1065.
14. M. Kholghy, M. Saffaripour, C. Yip and M. J. Thomson, *Combust. Flame*, 2013, **160**, 2119-2130.
15. A. D'Anna, A. Rolando, C. Allouis, P. Minutolo and A. D'Alessio, *P. Combust. Inst.*, 2005, **30**, 1449-1456.
16. A. D'Anna, M. Commodo, S. Violi, C. Allouis and J. Kent, *P. Combust. Inst.*, 2007, **31**, 621-629.
17. R. A. Dobbins, R. A. Fletcher and W. Lu, *Combust. Flame*, 1995, **100**, 301-309.
18. R. A. Dobbins, R. A. Fletcher and H.-C. Chang, *Combust. Flame*, 1998, **115**, 285-298.
19. R. A. Fletcher, R. A. Dobbins and H.-C. Chang, *Anal. Chem.*, 1998, **70**, 2745-2749.
20. S. E. Stein and A. Fahr, *J. Phys. Chem.*, 1985, **89**, 3714-3725.
21. A. L. Lafleur, K. Taghizadeh, J. B. Howard, J. F. Anacleto and M. A. Quilliam, *J. Am. Soc. Mass Spectr.*, 1996, **7**, 276-286.
22. A. Santamaría, N. Yang, E. Eddings and F. Mondragón, *Combust. Flame*, 2010, **157**, 33-42.
23. A. Santamaría, F. Mondragón, W. Quiñónez, E. G. Eddings and A. F. Sarofim, *Fuel*, 2007, **86**, 1908-1917.
24. L. G. Blevins, R. A. Fletcher, B. A. Benner Jr., E. B. Steel and G. W. Mulholland, *P. Combust. Inst.*, 2002, **29**, 2325-2333.
25. A. Santamaría, F. Mondragón, A. Molina, N. D. Marsh, E. G. Eddings and A. F. Sarofim, *Combust. Flame*, 2006, **146**, 52-62.
26. S. A. Skeen, H. A. Michelsen, K. R. Wilson, D. M. Popolan, A. Violi and N. Hansen, *J. Aerosol Sci.*, 2013, **58**, 86-102.
27. L. Wang, C. Song, J. Song, G. Lv, H. Pang and W. Zhang, *P. Combust. Inst.*, 2013, **34**, 3099-3106.
28. B. Öktem, M. P. Tolocka, B. Zhao, H. Wang and M. V. Johnston, *Combust. Flame*, 2005, **142**, 364-373.
29. B. Zhao, K. Uchikawa and H. Wang, *P. Combust. Inst.*, 2007, **31**, 851-860.
30. J. P. Cain, P. L. Gassman, H. Wang and A. Laskin, *Phys. Chem. Chem. Phys.*, 2010, **12**, 5206-5218.
31. J. P. Cain, J. Camacho, D. J. Phares, H. Wang and A. Laskin, *P. Combust. Inst.*, 2011, **33**, 533-540.

32. A. D. Abid, N. Heinz, E. D. Tolmachoff, D. J. Phares, C. S. Campbell and H. Wang, *Combust. Flame*, 2008, **154**, 775-788.
33. H. Wang, *P. Combust. Inst.*, 2011, **33**, 41-67.
34. R. A. Dobbins, *Aerosol Sci. Tech.*, 2007, **41**, 485-496.
35. P. J. Roach, J. Laskin and A. Laskin, *Analyst*, 2010, **135**, 2233-2236.
36. P. J. Roach, J. Laskin and A. Laskin, *Anal. Chem.*, 2010, **82**, 7979-7986.
37. S. A. Nizkorodov, J. Laskin and A. Laskin, *Phys. Chem. Chem. Phys.*, 2011, **13**, 3612-3629.
38. J. Laskin, A. Laskin, P. J. Roach, G. W. Slysz, G. A. Anderson, S. A. Nizkorodov, D. L. Bones and L. Q. Nguyen, *Anal. Chem.*, 2010, **82**, 2048-2058.
39. R. E. O'Brien, T. B. Nguyen, A. Laskin, J. Laskin, P. L. Hayes, S. Liu, J. L. Jimenez, L. M. Russell, S. A. Nizkorodov and A. H. Goldstein, *J. Geophys. Res.-Atmos.*, 2013, **118**, 1042-1051.
40. P. Lin, J. Z. Yu, G. Engling and M. Kalberer, *Environ. Sci. Technol.*, 2012, **46**, 13118-13127.
41. Ö. L. Gülder, D. R. Snelling and R. A. Sawchuk, *Symp. (Int.) Combust.*, 1996, **26**, 2351-2358.
42. Ü. Ö. Köylü, C. S. McEnally, D. E. Rosner and L. D. Pfefferle, *Combust. Flame*, 1997, **110**, 494-507.
43. M. R. Kholghy, "The evolution of soot morphology in laminar co-flow diffusion flames of the surrogates for jet A-1 and a synthetic kerosene," University of Toronto, 2012.
44. P. J. Roach, J. Laskin and A. Laskin, *Anal. Chem.*, 2011, **83**, 4924-4929.
45. P. A. Eckert, P. J. Roach, A. Laskin and J. Laskin, *Anal. Chem.*, 2011, **84**, 1517-1525.
46. V. V. Lobodin, A. G. Marshall and C. S. Hsu, *Anal. Chem.*, 2012, **84**, 3410-3416.
47. K. Siegmann and K. Sattler, *J. Chem. Phys.*, 2000, **112**, 698-709.
48. P. T. A. Reilly, R. A. Gieray, W. B. Whitten and J. M. Ramsey, *Combust. Flame*, 2000, **122**, 90-104.
49. M. Schenk, S. Lieb, H. Vieker, A. Beyer, A. Gölzhäuser, H. Wang and K. Kohse-Höinghaus, *ChemPhysChem*, 2013, **14**, 3248-3254.
50. M. Schenk, S. Lieb, H. Vieker, A. Beyer, A. Gölzhäuser, H. Wang and K. Kohse-Höinghaus, *P. Combust. Inst.*, 2014, in press.
51. S. Léonard, G. W. Mulholland, R. Puri and R. J. Santoro, *Combust. Flame*, 1994, **98**, 20-34.
52. M. E. Birch and R. A. Cary, *Aerosol Sci. Tech.*, 1996, **25**, 221-241.
53. M. Frenklach and H. Wang, *Symp. (Int.) Combust.*, 1991, **23**, 1559-1566.
54. A. Kazakov, H. Wang and M. Frenklach, *Combust. Flame*, 1995, **100**, 111-120.
55. B. Dellinger, S. Lomnicki, L. Khachatryan, Z. Maskos, R. W. Hall, J. Adounkpe, C. McFerrin and H. Truong, *P. Combust. Inst.*, 2007, **31**, 521-528.
56. E. Dames, B. Sirjean and H. Wang, *J. Phys. Chem. A*, 2009, **114**, 1161-1168.
57. G. L. Squadrito, R. Cueto, B. Dellinger and W. A. Pryor, *Free Radical Bio. Med.*, 2001, **31**, 1132-1138.
58. K. Siegmann, H. Hepp and K. Sattler, *Combust. Sci. Technol.*, 1995, **109**, 165-181.

Figure Captions

Figure 1. Illustrations of the progression of liquid-like and the carbonization soot particles detected along the centerline of the flame reported by Kholghy *et al.*[14] The dark solid lines are rough illustration of the luminous zone of the flame, and the light solid lines are illustration of the inner region of the flame where soot particles have been measured by TEM but not by light extinction.

Figure 2. The burner and fuel vaporization system.

Figure 3. Nano-DESI/HR-MS mass spectra of soot samples collected along the centerline of the flame as a function of the distance from the burner exit.

Figure 4. Variation of the number of hydrogen atoms with the number of carbon atoms in species detected by nano-DESI/HR-MS, as a function of the distance from the burner exit. The symbol size is proportional to the logarithm of the peak intensity. Limiting cases are also shown for aliphatic hydrocarbons (blue line) and *cata*-condensed (less compact) and *peri*-condensed (circular, most compact structures) PAHs (red lines).[58] Black dashed line of $H = 1.25\ C + 2.5$ is used to distinguish roughly between "aromatic CHO" (red symbols below that line) and "aliphatic CHO" (blue symbols above that line) species.

Figure 5. Histograms of number of carbon atoms (left), H/C ratios (middle) and O/C ratios (right) characteristic for "aromatic CHO" (red) and "aliphatic CHO" (blue) species detected in the samples at different heights. The bars indicate counting statistics based on the number of detected CHO species, and symbols connected by lines exhibit summed intensity of corresponding peaks in the mass spectra.

Figure 6. H/C atomic ratios in CHO species detected in samples collected at selected distances from the burner exit. The symbol colors denote the number of H atoms in the species. The symbol size is proportional to the logarithm of the MS peak intensity. The dashed line represents the separation of the aliphatic and aromatic components, defined as $H = 1.25\ C + 2.5$.

Figure 7. Variation in double bound equivalent (DBE) values with the number of carbon atoms in CHO species. Values are shown as a function of the distance from the burner exit, and the symbol size is proportional to the logarithm of the peak intensity. Symbol colors indicate the H/C ratio. DBE limits of *cata*- and *peri*-condensed PAHs are shown for reference along with the maximum DBE values suggested by Lobodin *et al.*[46]

685 **Figure 8**. O/C atomic ratios in CHO species detected in samples collected at selected distances
686 from the burner exit. The symbol colors denote the number of H atoms in the
687 species. The symbol size is proportional to the logarithm of the MS peak intensity.

688 **Figure 9**. Van Krevelen plot showing H/C-versus-O/C atomic ratios in CHO species detected
689 in samples collected at selected distances from the burner exit. The symbol colors
690 denote the number of C atoms in the species. The symbol size is proportional to the
691 logarithm of the MS peak intensity.

692 **Figure 10**. Selected, plausible PAH structures as detected by nano-DESI/HR-MS.

693 **Figure 11**. Key gas-phase species computed along the centerline of the flame.[6]
694

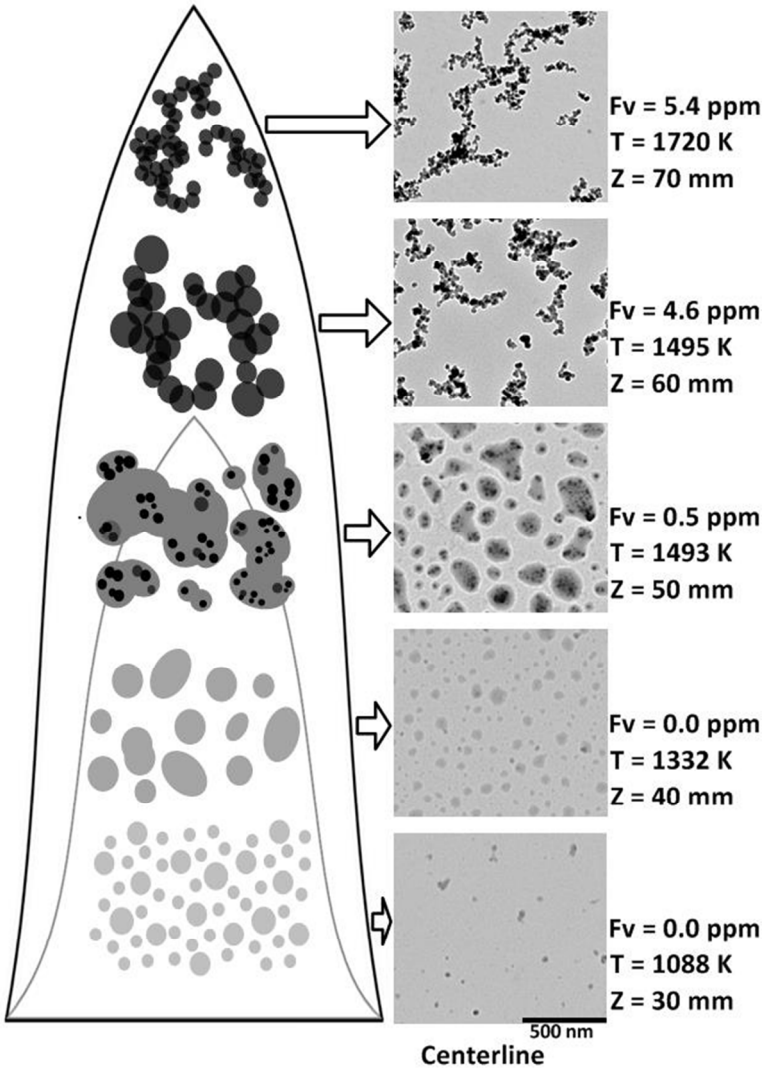

Figure 1. Illustrations of the progression of liquid-like and the carbonized soot particles detected along the centerline of the flame reported by Kholghy *et al.*[14] The dark solid lines are rough illustration of the luminous zone of the flame, and the light solid lines are illustration of the inner region of the flame where soot particles have been measured by TEM but not by light extinction.

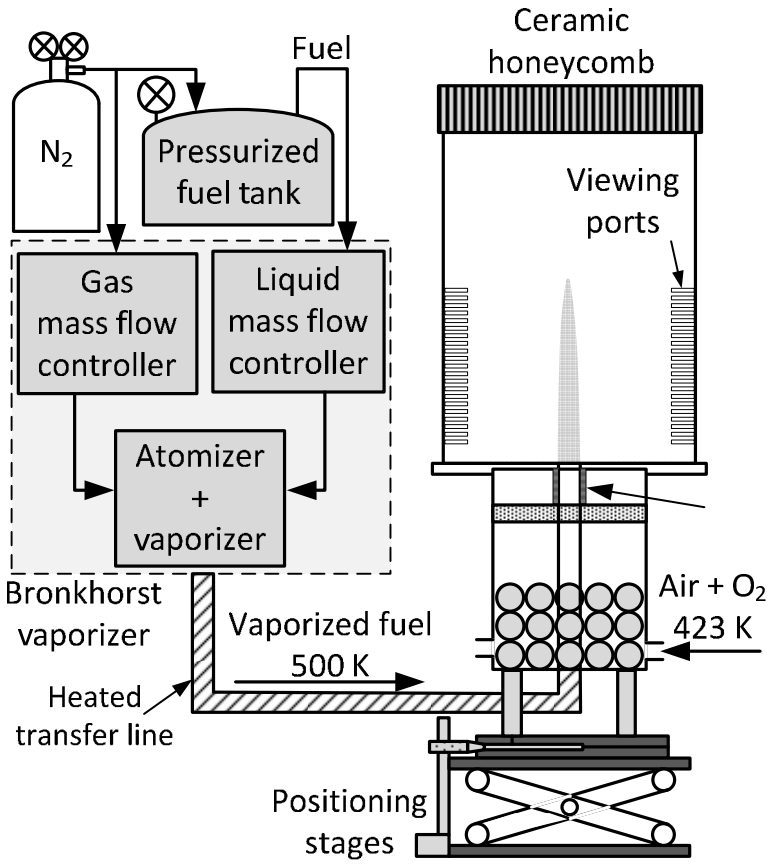

Figure 2. The burner and fuel vaporization system.

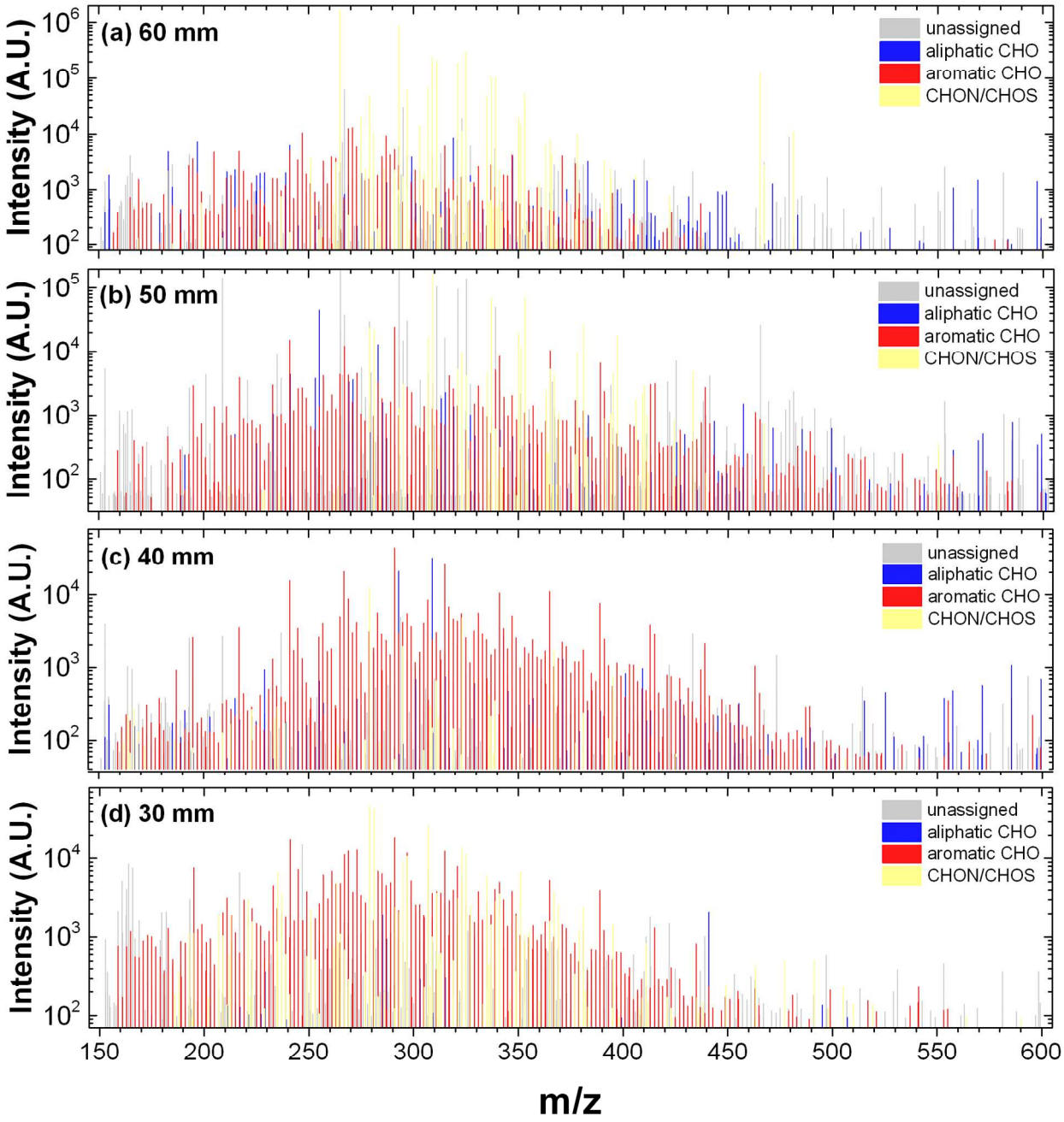

Figure 3. Nano-DESI/HR-MS mass spectra of soot samples collected along the centerline of the flame as a function of the distance from the burner exit.

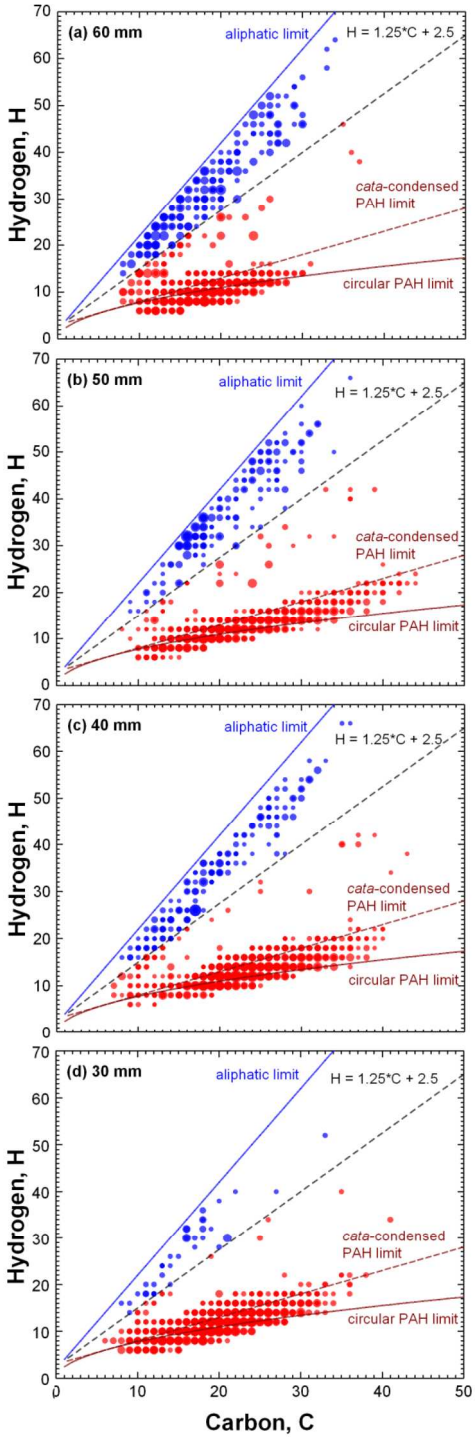

Figure 4. Variation of the number of hydrogen atoms with the number of carbon atoms in species detected by nano-DESI/HR-MS, as a function of the distance from the burner exit. The symbol size is proportional to the logarithm of the peak intensity. Limiting cases are also shown for aliphatic hydrocarbons (blue line) and *cata*-condensed (less compact) and *peri*-condensed (circular, most compact structures) PAHs (red lines).[58] Black dashed line of $H = 1.25\ C + 2.5$ is used to distinguish roughly between "aromatic CHO" (red symbols below that line) and "aliphatic CHO" (blue symbols above that line) species.

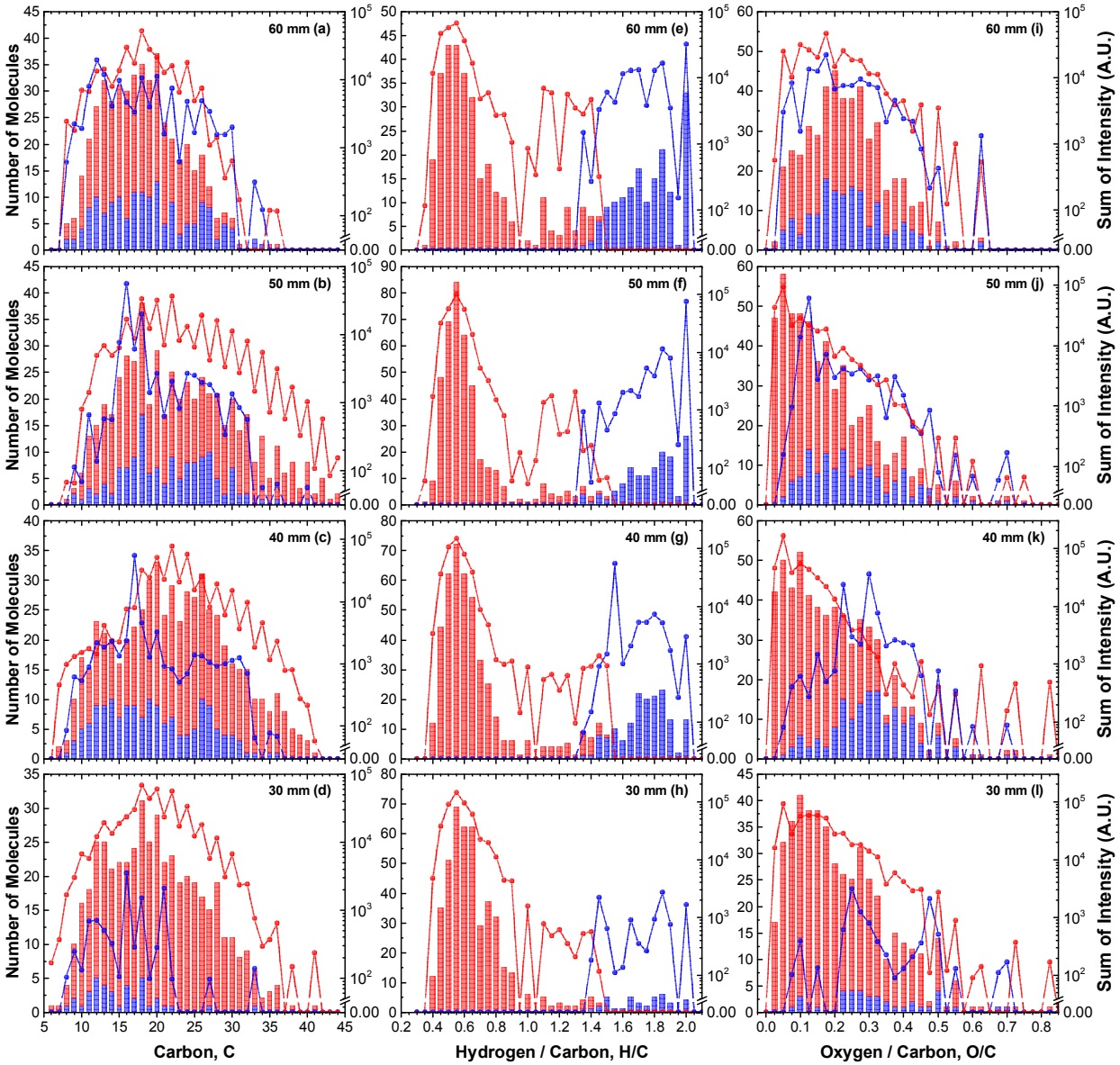

Figure 5. Histograms of number of carbon atoms (left), H/C ratios (middle) and O/C ratios (right) characteristic for "aromatic CHO" (red) and "aliphatic CHO" (blue) species detected in the samples at different heights. The bars indicate counting statistics based on the number of detected CHO species, and symbols connected by lines exhibit summed intensity of corresponding peaks in the mass spectra.

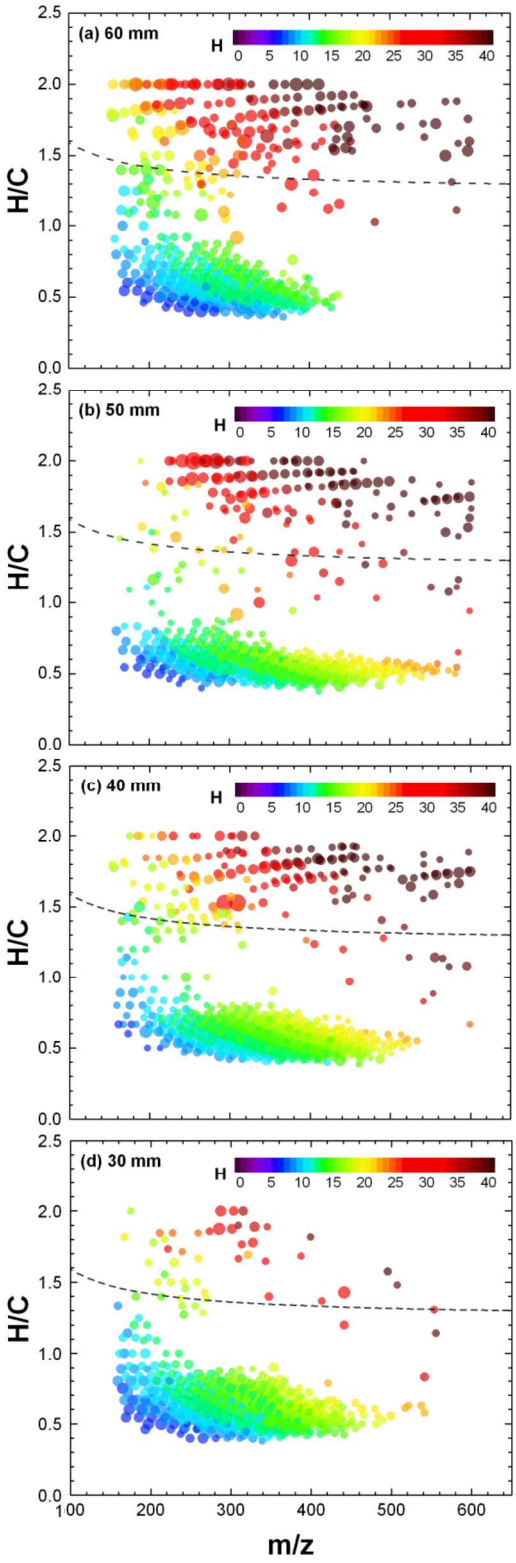

Figure 6. H/C atomic ratios in CHO species detected in samples collected at selected distances from the burner exit. The symbol colors denote the number of H atoms in the species. The symbol size is proportional to the logarithm of the MS peak intensity. The dashed line represents the separation of the aliphatic and aromatic components, defined as $H = 1.25\ C + 2.5$.

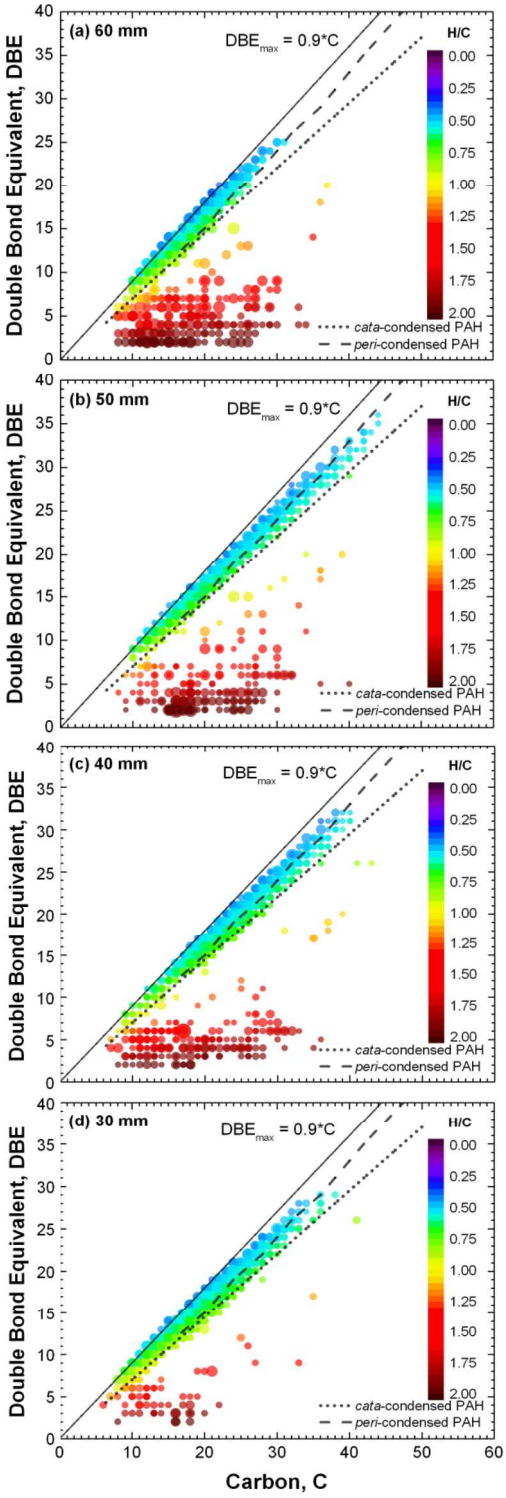

Figure 7. Variation in double bound equivalent (DBE) values with the number of carbon atoms in CHO species. Values are shown as a function of the distance from the burner exit, and the symbol size is proportional to the logarithm of the peak intensity. Symbol colors indicate the H/C ratio. DBE limits of *cata*- and *peri*-condensed PAHs are shown for reference along with the maximum DBE values suggested by Lobodin *et al.*[46]

745

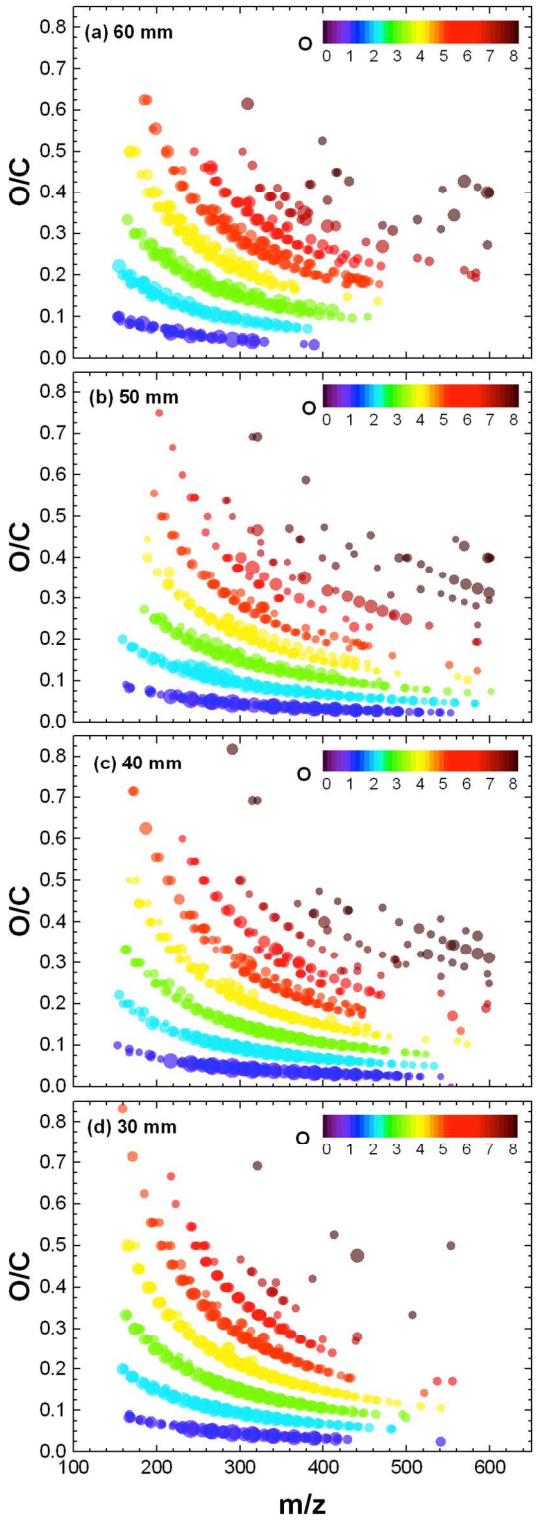

746

747 **Figure 8**. O/C atomic ratios in CHO species detected in samples collected at selected distances from
748 the burner exit. The symbol colors denote the number of H atoms in the species. The symbol size is
749 proportional to the logarithm of the MS peak intensity.

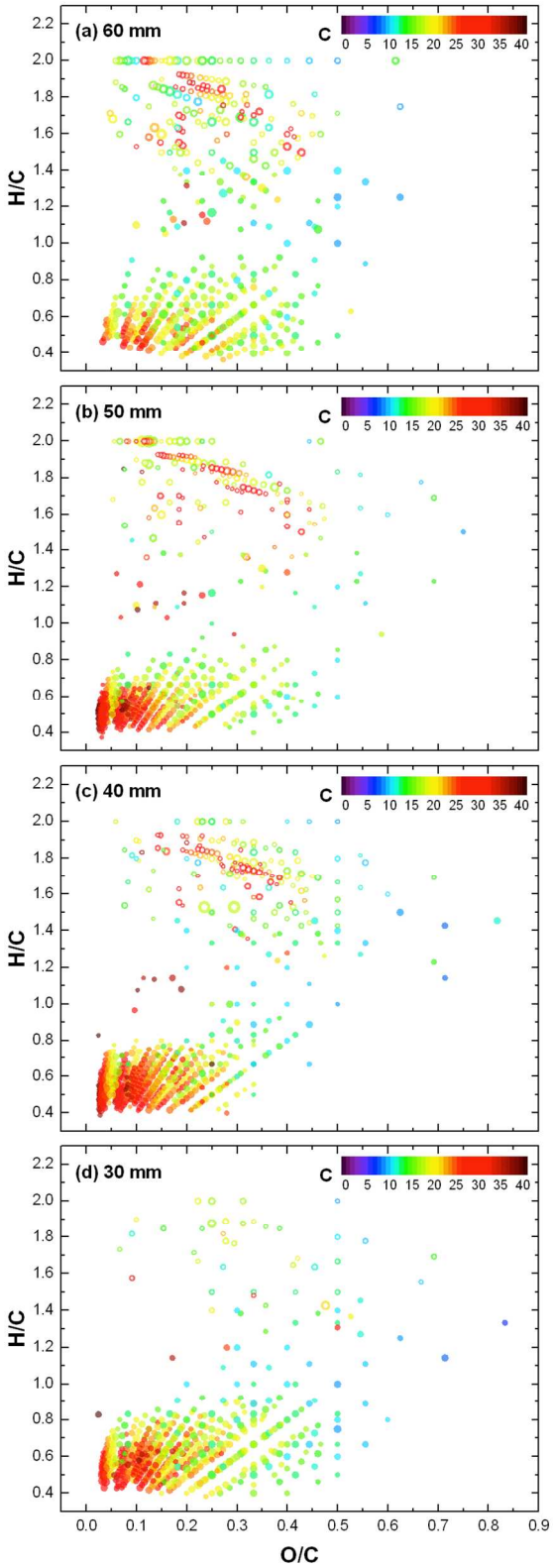

Figure 9. Van Krevelen plot showing H/C-versus-O/C atomic ratios in CHO species detected in samples collected at selected distances from the burner exit. The symbol colors denote the number of C atoms in the species. The symbol size is proportional to the logarithm of the MS peak intensity.

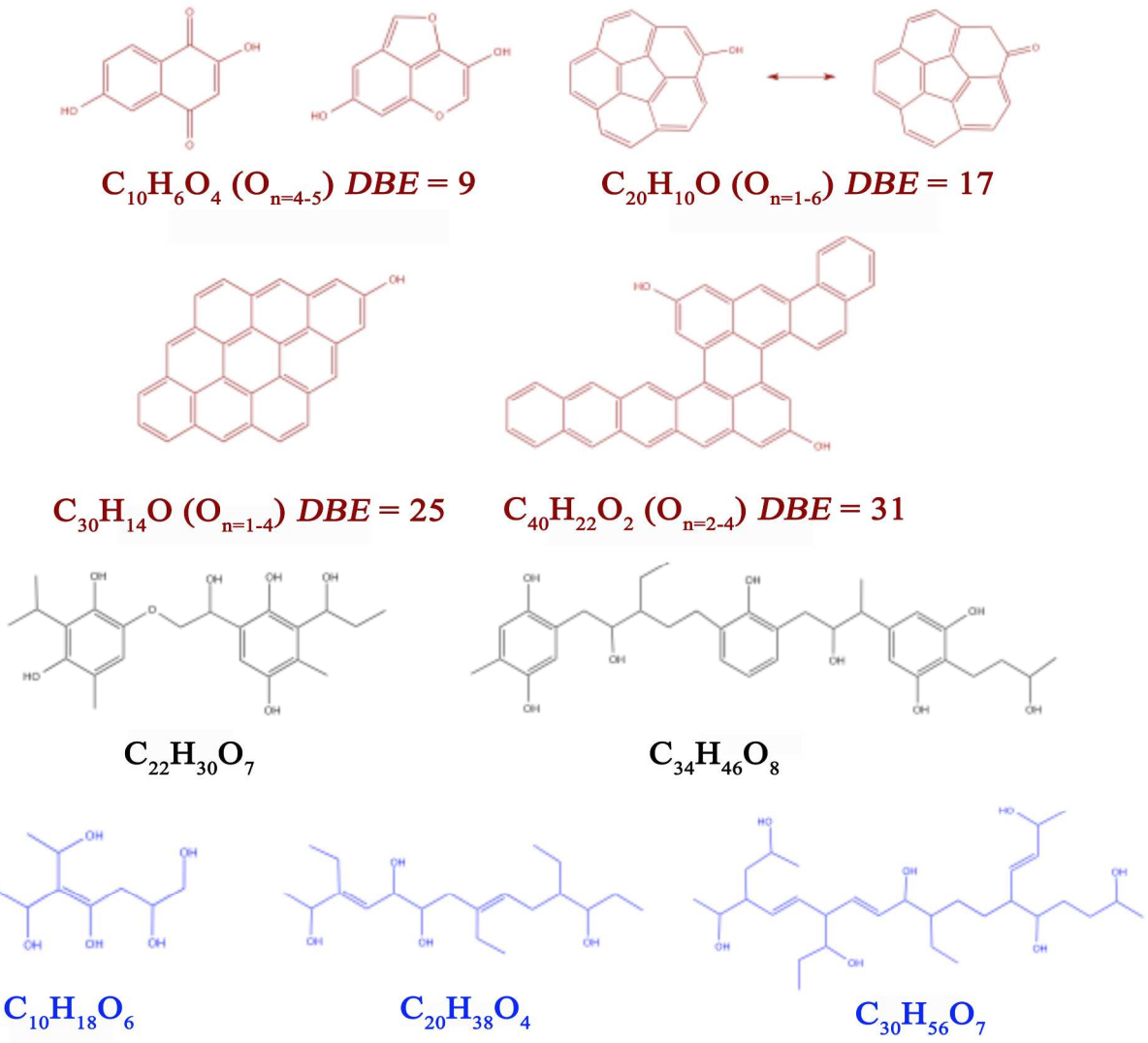

754
755 **Figure 10**. Selected, plausible PAH structures as detected by nano-DESI/HR-MS.
756

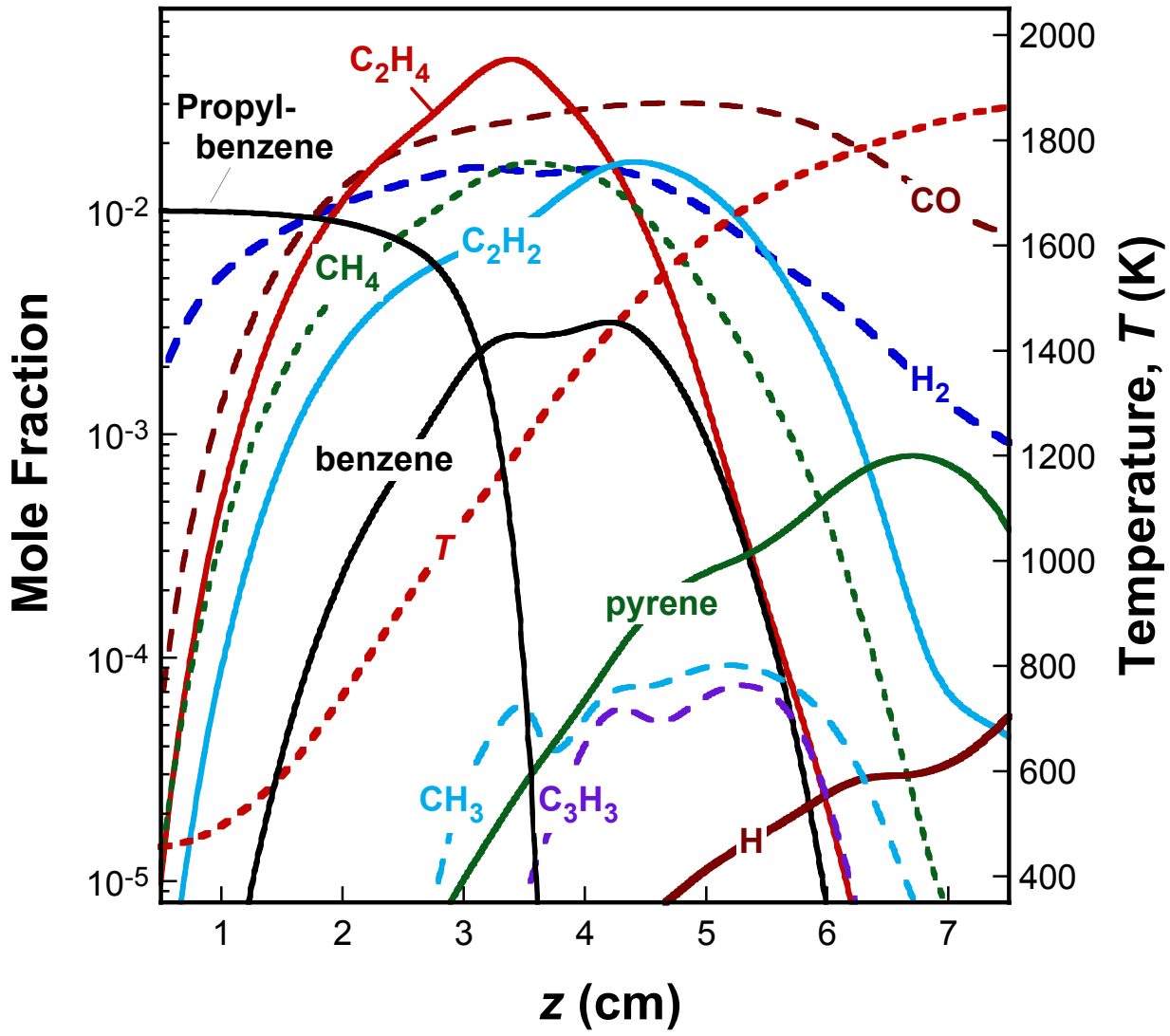

Figure 11. Key gas-phase species computed along the centerline of the flame.[6]